





Article

Agricultural Wastewater Treatment Using Oil Palm Waste Activated Hydrochar for Reuse in Plant Irrigation: Synthesis, Characterization, and Process Optimization

Ahmad Hussaini Jagaba ^{1,2,*} , Faizah Mohammed Bashir ^{3,*}, Ibrahim Mohammed Lawal ^{2,4} , Abdullahi Kilaco Usman ⁵ , Nura Shehu Aliyu Yaro ^{1,6} , Abdullahi Haruna Birniwa ⁷, Haifa Youssef Hamdoun ³ and Nahla M. Shannan ⁸

¹ Department of Civil and Environmental Engineering, Universiti Teknologi PETRONAS, Bandar Seri Iskandar 32610, Malaysia

² Department of Civil Engineering, Abubakar Tafawa Balewa University, Bauchi 740272, Nigeria

³ Department of Decoration and Interior Design, University of Hail, Hail 55467, Saudi Arabia

⁴ Department of Civil and Environmental Engineering, University of Strathclyde, Glasgow G4 0RE, UK

⁵ School of Civil Engineering, Universiti Teknologi Malaysia, Johor Bahru 81310, Malaysia

⁶ Department of Civil Engineering, Ahmadu Bello University, Zaria 810107, Nigeria

⁷ Department of Chemistry, Sule Lamido University, Kafin-Hausa PMB 048, Nigeria

⁸ Program in Electronics and Telecommunications Engineering Technology, Applied College, University of Hail, Hail 55467, Saudi Arabia

* Correspondence: ahjagaba@atbu.edu.ng (A.H.J.); fai.bashir@uoh.edu.sa (F.M.B.)



Citation: Jagaba, A.H.; Bashir, F.M.; Lawal, I.M.; Usman, A.K.; Yaro, N.S.A.; Birniwa, A.H.; Hamdoun, H.Y.; Shannan, N.M. Agricultural Wastewater Treatment Using Oil Palm Waste Activated Hydrochar for Reuse in Plant Irrigation: Synthesis, Characterization, and Process Optimization. *Agriculture* **2023**, *13*, 1531. <https://doi.org/10.3390/agriculture13081531>

Academic Editors: Ademola Ajayi-Banji and Andreas Gronauer

Received: 29 May 2023

Revised: 19 July 2023

Accepted: 25 July 2023

Published: 1 August 2023



Copyright: © 2023 by the authors. Licensee MDPI, Basel, Switzerland. This article is an open access article distributed under the terms and conditions of the Creative Commons Attribution (CC BY) license (<https://creativecommons.org/licenses/by/4.0/>).

Abstract: The best possible use of natural resources and the large amounts of trash produced by industrial and human activity is necessary for sustainable development. Due to the threat of global climate change and other environmental challenges, waste management systems are changing, leading to more instances of water resource management. The waste generated must be controlled from a sustainability point of view. Typically, the conventional disposal of Agricultural Wastewater (AW) and biomass can be achieved by recycling, reusing, and converting them into a variety of green products. To improve the AW quality for the purposes of environmental sustainability, Sustainable Development Goals (SDGs) 6 and 14, dealing with clean water, sanitation, and life below water, are very important goals. Therefore, the present investigation evaluates the effectiveness of a Bench-scale Activated Sludge Reactor (BASR) system for AW treatment. The BASR was designed to focus on getting the maximum possible utilization out of a biosorbent derived from oil palm waste activated hydrochar (OPAH). This is in accordance with SDG 9, which targets inorganic and organic waste utilization for added value. An experiment was developed using the Response Surface Methodology (RSM). A Hydraulic Retention Time (HRT) of 1–3 days was used in the bioreactor's setup and operation, and Mixed Liquor Suspended Solids (MLSS) concentrations of 4000–6000 mg/L were used. BASR was fed with AW with initial mean concentrations of 4486 ± 5.63 mg/L and 6649 ± 3.48 for the five-day Biochemical Oxygen Demand (BOD₅) and Chemical Oxygen Demand (COD) experiments, respectively. The results obtained showed that maximum reductions of 84.66% and 72.07% were recorded for BOD₅ and COD, respectively. Through RSM optimization, the greatest reductions in the amounts of organic materials were achieved with a 2-day HRT and an MLSS dosage of 5000 mg/L. Substrate elimination thresholds were assessed using the first-order, the Grau second-order, and the modified Stover–Kincannon models. The reported observations were found to be perfectly fit by the modified Stover–Kincannon model, with high R² values of 0.9908 and 0.9931 for BOD₅ and COD, respectively. As a result, the model may be used to design the BASR system and forecast how the reactor would behave. The findings from this study suggest that the developed OPAH has promising potential to be applied as eco-friendly material for the removal of BOD₅ and COD from AW. Consequently, the study findings additionally possess the ability to address SDGs 6, 9, and 14, in order to fulfil the United Nations (UN) goals through 2030.

Keywords: hydrochar; agricultural wastewater; kinetic modeling; oil palm waste; response surface methodology; waste management

1. Introduction

Agricultural wastewater (AW) is the excess water that runs off the field at the bottom of furrows, boundary strips, basins, and flooded areas during surface irrigation [1]. AW might also include effluent from plant processing field crops, as well as those for making processed food, both of which are operated by and for farmers, usually in centralized facilities. These kinds of plants produce a significant quantity of AW, collected through properly designed channels and pipes, and deposited either in a pond or a storage tank [2]. AW is one of the biggest contributors to global industrial pollution. Although the source of the raw materials, and the nature of the products, operations, and processing steps all have an impact on the composition and quantity of AW, it typically contains a significant number of organic materials, with high levels of chemical oxygen demand (COD) and total suspended solids (TSS), which have the potential to result in serious pollution issues [3]. If AW is released untreated into the environment, it will undoubtedly result in serious environmental issues. Regulations therefore call for the treatment of AW prior to discharge into the environment. AW treatment is regarded as one of the most difficult areas in environmental conservation [4,5]. The development of reasonable, integrated, cheap, and efficient techniques and technologies is a fundamental challenge in AW treatment [6]. A variety of strategies have been tried for AW treatment, with varying degrees of efficacy. Physicochemical processes are used to remove organic matter, nutrients, and refractory materials from AW [7,8]. Numerous methods, including coagulation–flocculation, adsorption, ion exchange, precipitation, photocatalytic degradation, membrane filtration, solvent extraction, catalytic oxidation, electrochemical oxidation, etc., have been tried and tested to remove these organic contaminants from water. However, the primary issue with most of the above-mentioned solutions is the restriction of the footprint on the current wastewater treatment plant [9]. Biological methods may be a good choice, but it is impossible to reach the regulatory limitations of discharge for this effluent with current procedures [10]. Scientists have been paying close attention to the use of combined activated sludge and biosorption techniques since waste management systems began to change globally owing to the imminent danger of global climate change and other environmental challenges [11,12].

In recent times, the biosorption method has attracted attention as a remedy for AW [13]. The different biosorbent materials for contaminant removal and resource recovery ranging from but not limited to raw and processed materials such as biochar, pyrochar, and hydrochar [14]. A growing interest is being shown in using agricultural materials such as oil palm waste for biosorption during wastewater treatment due to its remarkable chemical composition, wide availability, affordability, and renewability [15]. These wastes are also utilized as feedstock in thermochemical processes including hydrothermal carbonization. As a result, “Hydrochar” is produced, which is a more environmentally friendly biosorbent. The redirection of agricultural waste into hydrochar production with very high contaminant biosorption capacity could add to their value. The optimization of biosorption parameters needs to be applied. Thus, these optimization techniques pave the way for the biosorption process to evolve into an intriguing, sustainable, and affordable technology that produces low by-product levels and high-performance efficiency. The proper use of the response surface methodology (RSM) could lead to excellent design and optimization of AW biosorption processes [16]. This tool applies mathematical and statistical modeling techniques to estimate and optimize essential parameters that influence the biosorption process under various situations while treating AW [17].

There is indeed insufficient knowledge of the impact of biosorbents on organic matter removal in combined biosorption and activated sludge treatment systems. Thus, the objectives of this study are to: (i) synthesize and characterize activated hydrochar produced

from oil palm wastes (OPAH); (ii) optimize the bioreactor efficiency through RSM by analyzing the influence of mixed liquor suspended solids (MLSS) and hydraulic retention time (HRT) on BOD₅ and COD removal; (iii) develop kinetic models for the prediction of BOD₅ and COD removal rate; and (iv) determine the microbial community present in the system.

2. Materials and Methods

2.1. Materials

All the chemicals used in the experiment were of analytical grade and used as received with no purification required. The 600 L of AW that was used was supplied by a local palm oil mill agricultural company located in Malaysia. The AW sample was gathered in a sufficient quantity and preserved in a cold room. Before being employed in the reactor system, the obtained AW sample underwent characterization. The oil palm empty fruit bunches (PFB) shown in Figure S1a were acquired from a local company located in the nearby local market that processes oil palm waste. Before processing, the collected PFB samples were kept at 4 °C. The samples were washed repeatedly with tap water to remove any adherent contaminants that may have developed during processing. The collected samples were individually immersed in 1 L/100 g of distilled water for 24 h. The specimens were then dehydrated in an oven for 24 h at 110 °C after being rinsed with 0.5 L/100 g of acetone. They were then cleaned in deionized water and dried in an oven for 24 h at 105 °C. After drying, the size of the sample was initially reduced to 3–5 mm using a mechanical granulator. PFB was then ground to a 75 m powder using a mechanical grinder.

2.2. OPAH Biosorbent Preparation

Ten grams of dry PFB powder and 400 mL of ultrapure water were added to a stainless-steel reactor to produce the hydrochar shown in Figure S1b. The reactor was then heated to 150 °C and kept there for 8 h. After that, the reactor was cooled to ambient temperature before the hydrochar was thoroughly washed and dried for 12 h at 80 °C [18]. Apart from using 0.1 M of potassium hydroxide (KOH) solution in place of ultra-pure water, the process for producing activated hydrochar was essentially the same as that described above. The specimen was stored for a full day. After reaching a neutral pH, the activated adsorbent was rinsed with distilled water, tested with a digital pH meter, and dried at 110 °C. The pure hydrochar and the KOH-activated hydrochar had solid yields of 63 and 81%, respectively.

2.3. OPAH Characterization

The KBr pellet method [19] was utilized to assess the materials using a Varian 3100 Fourier-transform infrared (FTIR) spectroscope of the type (NICOLET iS10, Thermo Scientific, Waltham, MA, USA). Ni-filtered Cu K radiation with a graphite monochromator ($\lambda = 1.5406 \text{ \AA}$) at an angle 2θ of 0–80° was used to determine the mineral composition and crystallinity of the biosorbent. Field emission scanning electron microscopy (FESEM) of the OPAH was performed on (Carl-Zeiss AG, Oberkochen, Germany). High-resolution micrographs of the FESEM images were captured at a variety of k_x magnifications and an acceleration voltage of 200 kV. For nitrogen adsorption–desorption studies at 77 K, the specific surface area and pore size distribution of OPAH were measured on Gemini VII 2390, USA. The tests for moisture content, greater heating value, ultimate analysis, and proximal value were performed in accordance with American Society for Testing and Materials (ASTM) E1755-01, D4809-00, D3176-09, and E871-82, respectively [20–23].

2.4. BASR System Operation

The BASR shown in Figure S2 is a biological reactor made of 5 mm thick acrylic glass. It comprises an aeration tank, a clarifier, a storage tank for the effluent, and a significant number of tube diffusers installed. To improve the mixing of the entire liquid volume, horizontal air tube diffusers were installed at the reactor base to give oxygen in an up-flow

pattern. Thus, the biomass might receive adequate aeration. A peristaltic pump with a variable flow rate was also present, for reactor feeding. The goal was to adjust the reactor’s flowrate as needed. The bottom and top influent and effluent points, respectively, were in opposing directions. In the trial, baffles were utilized to stop biomass from washing into the effluent unit. 7.5 L of influent AW was continuously supplied into the 10 L capacity bioreactor using a peristaltic pump. Temperature, pH, and DO were roughly constant throughout the tests at $T = 24 \pm 3 \text{ }^\circ\text{C}$, $\text{pH} = 8.02 \pm 0.75$, $\text{DO} = 2.0 \pm 0.5 \text{ mg/L}$, respectively. Continuous measurements were made of the BOD₅, COD, MLSS, and mixed liquor volatile suspended solids (MLVSS). To investigate its effect on the management of AW, the BASR was performed with the inclusion of OPAH. Biomass stabilization was the main goal of the adaptation period. To achieve this, a maximum of 20 days was sufficient. The second acclimatization phase, during which the reactor received 2000 mg/L of biosorbent. The biosorbents were acclimated for ten days.

2.5. BASR Optimization by RSM for BOD₅ and COD Removal

RSM is a widely used optimization technique in many industrial processes, including chemical engineering, wastewater treatment, biotechnology, food chemistry, and material science [24]. It provides information on direct, pairwise interaction, and curvilinear variable impacts on a certain response. It is also a cost-effective method for quantifying the individual and interaction effects of process parameters, even in the presence of complex interactions, as well as predicting the optimum response parameter values within the experimental range of investigation [25]. The first step of RSM requires the selection of the specific design. RSM uses an experimental design to fit a model using the least squares technique. Analysis of variance (ANOVA) is used to reflect significant quadratic models and graphically analyze the data to obtained. The range and level of variables are presented in coded units. The interaction among the considered factors with the response are mostly shown in three dimensional plots. The coefficient of determination R² expresses the correctness and quality of the fit polynomial model, and the Fisher F-test in just the same application checks its statistical significance. The p value (probability) is used to choose or reject model terms. The contour plots are created using the impacts of the factors being researched. The optimum region for maximum contaminant removal, as well as the maximum biodegradability index could be identified based on the primary characteristics in the contour plots. Central Composite Design (CCD) is the most popular and applies proper assumptions to discover a true relationship between the collection of variables.

In this study, the effect of HRT (1-3 days) and MLSS (4000–6000 mg/L) concentration were investigated as process variables. The design matrix and outcomes produced using CCD in the experiment are shown in Table 1. The activities of BOD₅ and COD removal were used to evaluate the model’s performance. As a result, a quadratic equation, as defined in Equations (1) and (2), is used to describe the linear model.

$$y = f(m) \tag{1}$$

$$f(m) = \alpha_0 + \sum_{x=1}^z \alpha_x w_x + \sum_{i=1}^z \sum_{y \geq i}^z \alpha_{xy} w_x w_y + \delta \tag{2}$$

Table 1. BOD₅ and COD removal from AW using RSM matrix for optimization.

| Independent Variables | Symbol | Ranges of Variables and Codes | | |
|-----------------------|----------------|-------------------------------|------|------|
| | w | −1 | 0 | +1 |
| HYRT (days) | w _x | 1 | 2 | 3 |
| MLSS (mg/L) | w _y | 4000 | 5000 | 6000 |

2.6. Kinetic Study

2.6.1. The First-Order Kinetic Model

Equation (3) can be used to obtain the rate of change in substrate concentration in the BASR as follows:

$$\frac{N_i - N_o}{\theta} = B_1 N_o \quad (3)$$

By plotting $(N_i - N_o)/\theta$ versus N_o , the B_1 can be computed using the slope of the line.

The starting and effluent substrate contaminant concentrations [26] are N_i and N_o , the HRT is θ , and B_1 is the first-order substrate removal rate constant ($1/d$).

2.6.2. The Grau Second-Order Kinetic Model

The overall equation of the model, as rightly described by [27], can be written as Equation (4).

$$-\frac{dh}{dq} = S_c \cdot \left(\frac{N_o}{N_i}\right)^2 \quad (4)$$

Equation (5) can be produced by integrating Equation (4) and then scaling it:

$$\frac{N_i \nu}{N_i - N_o} = \nu - \frac{N_i}{S_c N_o} \quad (5)$$

where $S_c =$ second-order removal constant, ($1/d$).

$(N_i - N_o)/N_i$ exhibits the efficacy of pollutant removal. It is represented by the sign z . However, if the second element in the right half of Equation (5) is taken as a constant, Equation (4):

$$\frac{\nu}{z} = j + k \quad (6)$$

Plotting $\frac{\nu}{z}$ against ν , with the amounts of j and k being constant values, will yield the line's slope and intercept.

2.6.3. The Modified Stover–Kincannon Model

Adopted from the study reported in [28], the updated Stover–Kincannon model is as follows:

$$\frac{dh}{dq} = \frac{P}{M_x} (N_i - N_o) = \frac{C_t \left(\frac{PN_i}{M_x}\right)}{F_y + \left(\frac{PN_i}{M_x}\right)} \quad (7)$$

Equation (7) will be linearized to produce Equation (8):

$$\left(\frac{dh}{dq}\right)^{-1} = \frac{M_x}{P(N_i - N_o)} = \frac{F_y}{C_t} \left(\frac{M_x}{PN_i}\right) + \frac{1}{C_t} \quad (8)$$

where $C_t =$ max. COD and BOD₅ removal (g/L d), $F_y =$ saturation constant (g/L d).

By plotting $\frac{M_x}{P(N_i - N_o)}$ versus $\frac{M_x}{PN_i}$, slope = $\frac{F_y}{C_t}$, intercept = $\frac{1}{C_t}$.

2.7. Microbial Community Analysis

A small volume of the sample was taken from the aeration tank to be checked under microscopic lens to see the types of microorganisms exist in the aeration tank. The state of the microbial population in the activated sludge process will be monitored in detail as a result.

3. Results and Discussion

3.1. Characteristics of AW

The influent AW was examined physically and chemically. Table 2 shows its characteristics. It can be observed that the values of both BOD₅ and COD are above the standard

permissible limits. Due to the length of time this project took to complete, both substrates were collected twice during the experiment: once at the start of the study, and once when the digester started working at a 3-day HRT. AW and sewage sludge were both examined when they arrived at the lab.

Table 2. Physico-chemical characterization of AW.

| Parameters | Values | Standard A | Standard B |
|--|--------------|------------|------------|
| Temperature °C | 24.3 ± 0.71 | 40 | 40 |
| pH | 8.04 ± 0.65 | 6.0–9.0 | 5.5–9.0 |
| COD (mg/L) | 6649 ± 3.48 | 120 | 200 |
| BOD ₅ (mg/L) | 4486 ± 5.63 | 20 | 50 |
| NH ₄ ⁺ -N (mg/L) | 89.32 ± 7.19 | 10 | 20 |
| TDS (mg/L) | 1047 ± 6.43 | 200 | 600 |
| Total phosphorus (mg/L) | 291 ± 4.05 | 10 | 30 |
| EC (μS cm ⁻¹) | 1044 ± 1.00 | - | - |
| Suspended Solids (mg/L) | 387 ± 1.96 | 50 | 100 |
| Turbidity (NTU) | 349 ± 5.14 | 1 | 5 |
| Color (PtCo.) | 1572 ± 3.80 | ≤100 | ≤200 |

Key: ammonium (NH₄⁺-N); total dissolved solids (TDS); electrical conductivity (EC); nephelometric turbidity units (NTU); platinum–cobalt (PtCo).

3.2. Characterization of OPAH

The FESEM image in Figure 1 presents the morphology of the OPAH. The porous structure remains unchanged following carbonization, implying that pyrolysis does not significantly alter the structure of the precursor. The loss of water content and organic compounds due to decomposition could occur, leading to a decrease in mass. The images show that the surface of OPAH has been chemically functionalized with amine groups, producing a surface more suitable for base treatment. There is a drastic difference between the surface textures of OPAH before and after modification. Because of the presence of lignin and hemicellulose, the morphological appearance of OPAH is noticeable in the cross-section as consisting of surfaces with hard, cave-like, and even morphologies. The OPAH has a spongy porous structure, indicating that KOH promotes the formation of pores. Additionally, after meeting KOH, the biosorbent surface underwent modifications, as can be seen in the FESEM image, indicating the biosorption of contaminants. Following KOH treatment, the biosorbent surface appeared smooth and bright, indicating that the intended metals and functional groups on the surface underwent a physicochemical interaction that resulted in the development of flake-like deposits.

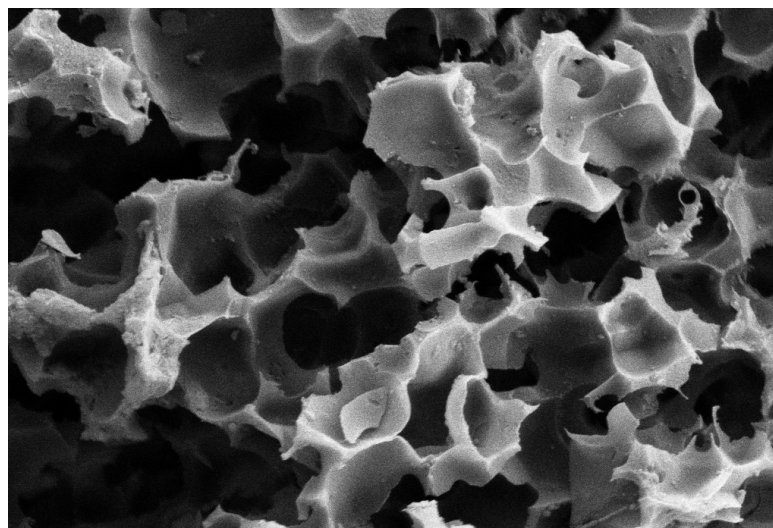


Figure 1. FESEM images of the OPAH at 2 μm.

The FTIR spectra of the functional groups of the OPAH are presented in Figure 2. The figure displays peaks that coincide with those already published [29,30]. The OPAH FTIR spectra exhibit multiple peaks, showing that it is made up of different chemical groups. The FTIR spectra of the OPAH exhibit decreased peak intensities, indicating that chemical groups were volatilized during pyrolysis; the results obtained correspond with a reduction in volatiles in biomass following pyrolysis. The strong and distinct peaks at 3698 cm^{-1} are caused by O-H stretching vibration. The peaks at 1627 cm^{-1} and 1495 cm^{-1} are attributable to C-H stretching vibrations. The absorption band corresponds to C=O stretching in the OPAH pores, as demonstrated by the peak at 1113 cm^{-1} . The presence of C=O and C=C bonds in the biomass supports the presence of lignin. The material contains the O-H group, as demonstrated by the strong, broad band at 471 cm^{-1} , which is due to C=C stretching vibration.

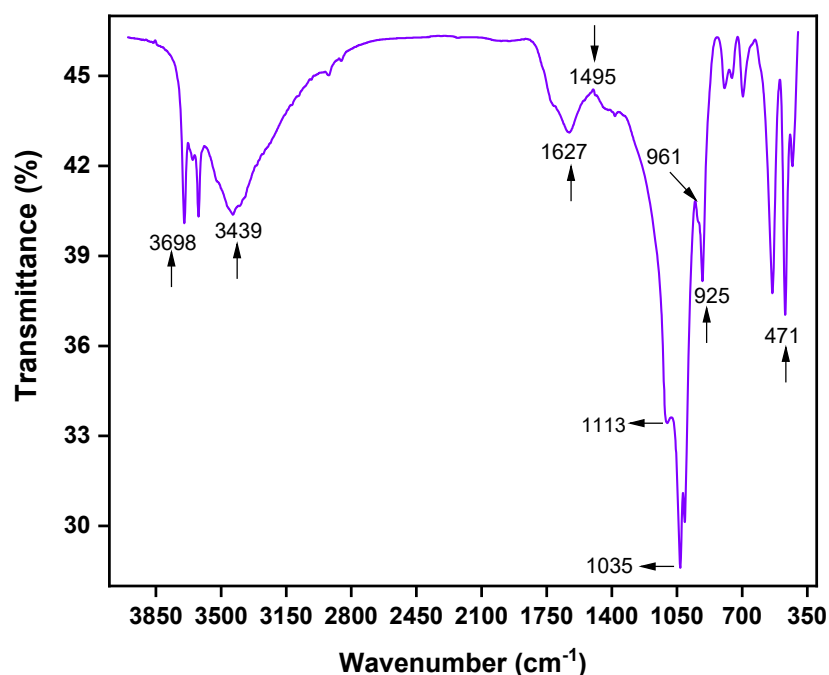


Figure 2. FTIR of OPAH.

The intense peaks observed at 1035 , 961 , and 925 cm^{-1} are caused by asymmetric and symmetric stretching and bending vibrations of the carboxylate group, which may operate as adsorption sites for target contaminants. When comparing these spectrum peaks, three peaks are shifted, and these will always be present for OPAH. Because the peaks were not compared between OPAH and other waste-derived hydrochars in this research, it is reasonable that the material arose in the peak of the oxygen-containing functional group, as the OPAH undergoes oxidation and is decreased by the ferrocene. When compared to other research, the small number of low-level peaks indicates the successful synthesis of OPAH.

The pH of a substance refers to a value on a numerical scale that is used to determine how acidic or basic a solution is, with a pH of 7 being neutral. The rate of adsorption is affected by the pH of the solution from which adsorption occurs. While hydrogen and hydroxide ions are heavily adsorbed, the pH of the solution influences the adsorption of other ions. The bulk of colored materials found in the industry are negatively charged; therefore, carbons will typically yield higher decolorization with increasing acidity of the solution; nevertheless, the pH of the adsorbent itself is a crucial consideration, since it may impact the pH of the liquid. The pH values measured are within the permitted range. Among the most important aspects in boosting the adsorptive power of a hydrochar is porosity. The porosity of a hydrochar is proportional to its bulk density and specific gravity. The number of pores in a sample is described by its porosity. As a result, higher porosities improve the

adsorbent's adsorption capability. Previous research has shown that the degree of adsorption increases as the surface area of the adsorbent increases. As a result, finely crushed metals and porous solids with large surface areas work effectively as adsorbents. The Brunauer–Emmett–Teller (BET) material surface area analysis and mean pore size, as shown in Table 3, are 774.08 m²/g and 1.192 nm, respectively. The substantially elevated BET value, which can be seen to possess a Type II nature at elevated relative pressure, shows an abundance of large-sized meso- and macro-pores that are not filled as saturation approaches.

Table 3. OPAH surface and structural properties.

| Parameter | pH | BET Surface Area (m ² /g) | Total Pore Volume (cm ³ /g) | Average Pore Radius (Å) | Average Pore Size (nm) |
|-----------|------|--------------------------------------|--|-------------------------|------------------------|
| Values | 7.16 | 774.08 | 0.489 | 89.26 | 1.192 |

The OPAH chemical make-up is presented in Table 4. Al₂O₃, SiO₂, and Fe₂O₃ together make up 60.2% of the OPAH. Cl and CaO were both present in the OPAH, accounting for 0.92% and 7.53%, respectively. As can be observed, SiO₂ is the ingredient that makes up the majority of OPAH. Material carbonization may be the cause of the high content (59.04%) of this ingredient. Thus, higher contents of SiO₂, K₂O, CaO, and P₂O₅ play major roles in improving biosorption behavior. The OPAH adsorbent maintained the structural integrity required for the desired application.

Table 4. Chemical composition (wt%) of OPAH.

| SiO ₂ | SO ₃ | CaO | P ₂ O ₅ | Al ₂ O ₃ | Fe ₂ O ₃ | K ₂ O | Rb ₂ O | MnO | MgO | Cl | Na ₂ O |
|------------------|-----------------|------|-------------------------------|--------------------------------|--------------------------------|------------------|-------------------|------|------|------|-------------------|
| 59.04 | 4.24 | 7.53 | 5.14 | 0.48 | 0.68 | 20.27 | 0.17 | 0.61 | 0.87 | 0.92 | 0.05 |

Key: silicon dioxide (SiO₂), sulfur trioxide (SO₃), calcium oxide (CaO), phosphorus pentoxide (P₂O₅), aluminum oxide (Al₂O₃), ferric oxide (Fe₂O₃), potassium oxide (K₂O), rubidium oxide (Rb₂O), manganese (II) oxide (MnO), magnesium oxide (MgO), chlorine (Cl), sodium oxide (Na₂O).

The proximate analysis, as shown in Table 5, revealed a low quantity of fixed carbon, ash, and volatile matter, implying that the particle density is comparatively low, and that the biomaterial would make a good raw material for bioreactor adsorbents. The ash present in the OPAH is a non-carbon addition that does not have a chemical relationship with the carbon surface. It is composed of different undesirable mineral compounds, the concentrations of which increase upon activation, ranging from 1 to 20%. A substantial moisture concentration is detrimental to hydrochar because it decreases carbon's mechanical strength and impairs its adsorptive activity. The addition of FC to hydrochar can boost its total activity. It also improves reactivation capacity; the higher the FC value, the more effectively the hydrochar will be able to serve as an adsorbent. Organic substances become fragile because of the heat that occurs during the carbonization and activation processes, leading molecules to break their bonds and connections [31].

Table 5. The proximate and ultimate analysis for OPAH.

| Ultimate and Proximate | (wt.%) |
|---------------------------------------|--------------|
| Proximate | |
| Fixed Carbon (FC) | 9.84 |
| Volatile Matter (VM) | 29.40 |
| Ash | 60.76 |
| Ultimate | |
| C | 67.08 |
| H | 4.39 |
| N | 8.26 |
| S | 0.95 |
| O | 19.32 |
| Experimental high heating value (HHV) | 3.95 (MJ/kg) |

Key: carbon (C), hydrogen (H), nitrogen (N), sulfur (S), oxygen (O).

Concerning the ultimate analysis for OPAH, also depicted in Table 5, the content values of carbon are in agreement with those of fixed carbon. There are some reports based on ultimate analysis for other kinds of materials. The difference between those results and those reported in this study could be due to the great difference between the properties of materials used as adsorbents and those of wastewater types.

3.3. BOD₅ and COD Removal

In this investigation, we examined how different HRT and MLSS concentrations affected the BASR's ability to remove BOD₅ and COD. The operational HRT was reduced over time from three days to two days to one day. The MLSS and MLVSS values at each HRT are listed in Table 6, as well as the operational length of the bioreactors, which ranged from 0 to 224 days. The bacteria incorporated in the biomass acclimated to the environment once the reactor was run up to a significantly stable state. The amounts of AW in the influent and effluent are also highlighted in Table 6. At the beginning of the experiment, it was noticeable that the reactor ran for 0 to 45 days.

Table 6. Steady-state conditions at three different HRTs.

| Parameters | HRT (d) | | | | | | | | |
|----------------------------------|---------|-------|-------|--------|---------|---------|---------|---------|---------|
| | 3 | 3 | 3 | 2 | 2 | 2 | 1 | 1 | 1 |
| Operational period (d) | 0–45 | 46–70 | 71–97 | 98–122 | 123–143 | 144–160 | 161–186 | 187–210 | 211–231 |
| Influent BOD ₅ (mg/L) | 4169 | 4293 | 4413 | 4029 | 4300 | 4365 | 4281 | 4220 | 4327 |
| Effluent BOD ₅ (mg/L) | 135 | 157 | 161 | 143 | 142 | 138 | 139 | 164 | 171 |
| Influent COD (mg/L) | 6025 | 6057 | 6084 | 6105 | 6067 | 6020 | 6023 | 6069 | 6103 |
| Effluent COD (mg/L) | 197 | 176 | 179 | 137 | 145 | 143 | 196 | 189 | 183 |
| MLVSS (mg/L) | 3139 | 3460 | 3231 | 2982 | 3405 | 3295 | 3358 | 3559 | 3735 |

Acclimatization took place over the first 15 days, and the 3-day HRT phase was administered over the following 30 days. In the BASR, microorganisms are immobilized on an inert support to reduce loss of biomass and increase bacterial activity. To assess the effectiveness of an industrial WWTP, BOD₅ and COD are essential metrics. To guarantee that the effluent of the WWTP complies with the discharge requirements, all WWTP must be designed in accordance with the desirable range of raw influent BOD₅ and COD [32,33]. In accordance with discharge standards A and B, as highlighted earlier in Table 2, it is shown in Table 6 that the COD influent and effluent for BASR systems are relatively steady, with an elevated COD removal effectiveness.

As can be seen from Table 6, the 2-day HRT had the lowest values of effluent COD, at 137, 145, and 143 mg/L, respectively. This implies that the removal efficiencies were higher than those attained during the 1-day and 3-day HRTs. Treatment using an upflow anaerobic sludge blanket (UASB) led to 75% COD removal using sugarcane bagasse, while paddy straw resulted in 90% COD reduction. Nevertheless, some inhibitory compounds remaining in the solution following pH adjustment necessitate dilution prior to treatment. Another study also found similar COD removal efficiencies greater than 90% across three seasons in a UASB plant handling industrial effluent. With 85% COD removal effectiveness at a loading of 30 kg COD/m³d, the mesophilically produced sludge used in UASB as a seeding material enables rapid startup and steady operation. In [34], thermophilic sludge was grown on sucrose for four months. After adaptation, the system was capable of handling large COD loadings (91.2 kg/m³d), and the effectiveness of COD removal was 71%. A thermophilic UASB reactor was used in another investigation that showed COD removal of 42–69% and over 80% BOD removal. The findings indicated a significant concentration of refractile chemicals in wastewater, which in turn had a negative effect on the microbial community in the sludge granules.

The content of BOD₅ measured in the influent and effluent fractions are shown in Table 6. The treatment with activated sludge decreased BOD₅ content by 84.66%. The

decrease was determined using the BOD₅ values of chemically measured sieved sample data. The chemicals may have been reduced to a more bioavailable state during filtering under high pressure, which could be one explanation for the significant degree of BOD₅ removal. Following filtration, the samples used for the BOD₅ tests were promptly frozen. Regarding the influent sample, the impact of freezing was examined. It seems likely that freezing altered the sample’s makeup and made it easier for bacteria to break it down. The impact of HRT on the BOD₅ readings revealed the existence of inhibitory compounds. The removal of chemicals harmful to bacteria is one probable rationale for the elevated levels of BOD₅ [35]. Heavy metals, cyanide, certain waste organics, and aluminum are toxic substances known to inhibit biological activity enough. Wood extracts may not only be harmful to aquatic life but may also limit biomass growth. Spikes in the concentration of resin acid can have an impact on the viability of biomass. Since the effluent is diluted many times before entering the water system, it is possible that there will be a corresponding increase in the BOD. Thus, the amount of oxygen consumed by natural water due to the effluent may be much greater than previously believed. In other words, if BOD₅ is calculated in the presence of bacterially hazardous chemicals, the BOD₅ values obtained will be far too low.

3.4. BASR Optimization by RSM

3.4.1. RSM Fitting

To investigate the interaction of the HRT and MLSS parameters, to forecast the optimal operating conditions and their impact on response, i.e., BOD₅ and COD removal, quadratic model equations generated by RSM were developed, as shown by Equations (9) and (10).

$$\text{BOD}_5 \text{ removal (\%)} = + 81.63 + 5.08A - 1.70B - 4.27AB - 5.24A^2 - 5.57B^2 \quad (9)$$

$$\text{COD removal (\%)} = + 68.03 + 2.80A - 1.61B - 1.17AB - 5.24A^2 + 0.1774B^2 \quad (10)$$

where A and B represent HRT and MLSS, respectively.

In Equations (9) and (10), the positive sign denotes a positive relationship between the component and adsorption capacity, whereas a negative sign denotes an antagonistic impact [36]. Real-world investigations were carried out under optimal conditions, and BOD₅ and COD removals were contrasted with projected values. BOD₅ and COD error percentages were 2.5% and 2%, respectively. In the scenario of tests involving biosorption parameters, it has been claimed that an error percentage of less than 10% is acceptable [17].

The coefficient estimates for BOD₅ and COD removals in the BASR system, as depicted in Table 7, show the anticipated change in the reaction for each unit change in the factor value, while all other variables remain unchanged.

Table 7. Coefficients for the responses expressed as coded factors.

| Factor | BOD ₅ | | | | | | COD | | | | | |
|----------------|----------------------|----|----------------|------------|-------------|--------|----------------------|----|----------------|------------|-------------|--------|
| | Coefficient Estimate | df | Standard Error | 95% CI Low | 95% CI High | VIF | Coefficient Estimate | df | Standard Error | 95% CI Low | 95% CI High | VIF |
| Intercept | 81.63 | 1 | 1.78 | 77.06 | 86.21 | | 68.03 | 1 | 2.76 | 60.94 | 75.12 | |
| A-HRT | 5.08 | 1 | 1.42 | 1.44 | 8.72 | 1.0000 | 2.80 | 1 | 2.19 | -2.84 | 8.45 | 1.0000 |
| B-MLSS | -1.70 | 1 | 1.42 | -5.34 | 1.94 | 1.0000 | -1.61 | 1 | 2.19 | -7.25 | 4.03 | 1.0000 |
| AB | -4.27 | 1 | 1.73 | -8.73 | 0.1889 | 1.0000 | -1.17 | 1 | 2.69 | -8.08 | 5.74 | 1.0000 |
| A ² | -5.24 | 1 | 2.18 | -10.84 | 0.3613 | 1.08 | -5.24 | 1 | 3.38 | -13.92 | 3.44 | 1.08 |
| B ² | -5.57 | 1 | 2.18 | -11.17 | 0.0313 | 1.08 | 0.1774 | 1 | 3.38 | -8.50 | 8.86 | 1.08 |

3.4.2. Surface Plots

To demonstrate the relationship involving every factor (HRT and MLSS) and the response, we also examined the impact caused by factor interactions when the other factors were kept constant [37]. Figure 3a–d depicts the use of the 3D surface and contour plots. Figure 3 shows the 3D plots of the association between HRT and MLSS on the elimination of BOD₅ and COD, whereas OPAH dosage was chosen as an actual factor (2 g/L) in

RSM. HRT was discovered to be the most important element in the lowering of BOD₅ and COD [38]. In Figure 3, the point of prediction revealed the maximum and minimum points for optimization within the experimental regions. The fitted response curve depicts the real surface of effect on the elimination of BOD₅ and COD [39]. The plot suggests that the optimal range of HRT administration might be within 1–2 days, with increased elimination at lower HRT [40]. Similarly, the MLSS range of 5000 mg/L was determined to be the best, despite its continually increasing. OPAH was found to be a successful biosorbent, with removal rates of 84.66% for BOD₅ and 72.07% for COD. The response peaks in Figure 3 indicate that the best circumstances for maximal response values in the design space are largely dependent on HRT and MLSS time [41,42].

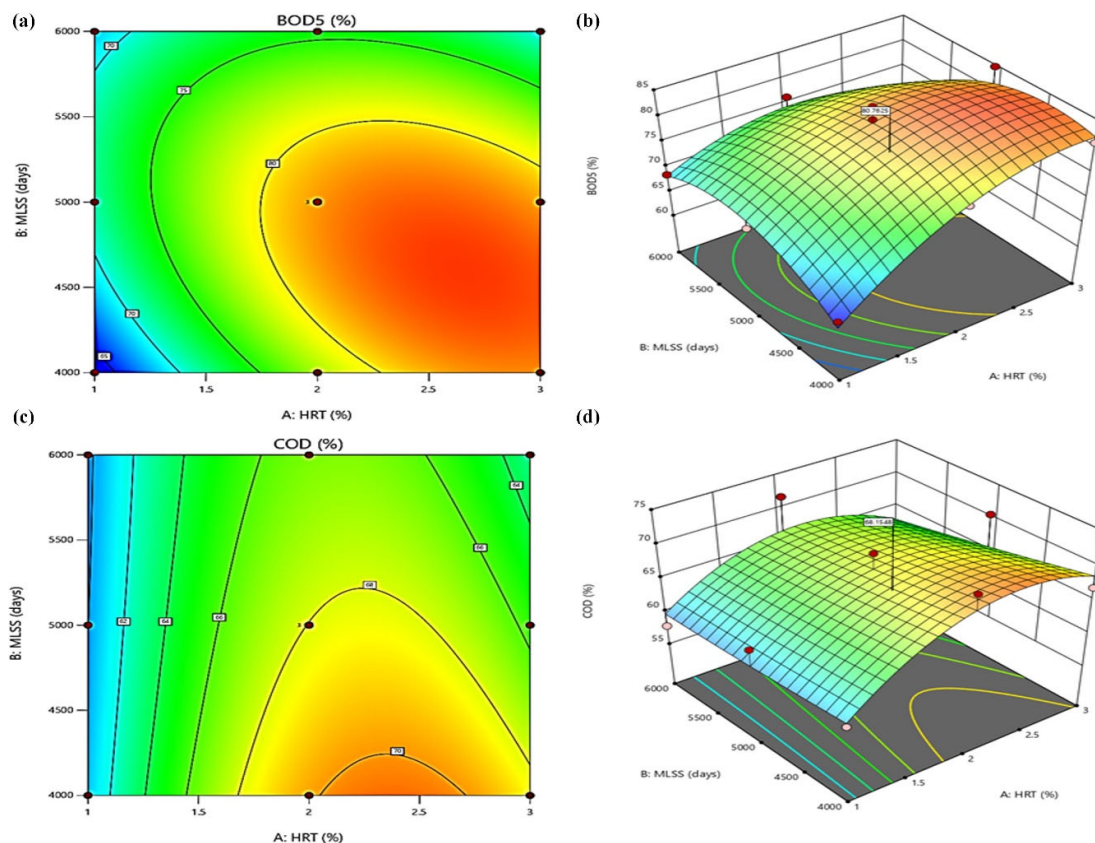


Figure 3. The contour and 3D plots for (a,b) BOD₅ removal (c,d) COD removal from the BASR.

3.4.3. Normal Residuals and Predicted versus Actual Plots of BASR System

The RSM output was utilized to verify the normality of the residuals, in addition to the expected and actual responses, as shown in Figure 4a–d. The anticipated and experimental outcomes were plotted to acquire a clearer idea of the models' prediction power [8]. The normal and residual capacities (Figure 4a,c) for BOD₅ and COD, respectively, were found to be in good agreement with each other, along with the actual and predicted biosorption capacities (Figure 4b,d). As can be seen, the two models were in good agreement with the experimental results. The BOD₅ and COD equation models were found to be suitable for use in this study. The quadratic model was found to be suitable, and the data points grouped together around the straight line, demonstrating a significant link between the experimental and predicted adsorption capacities.

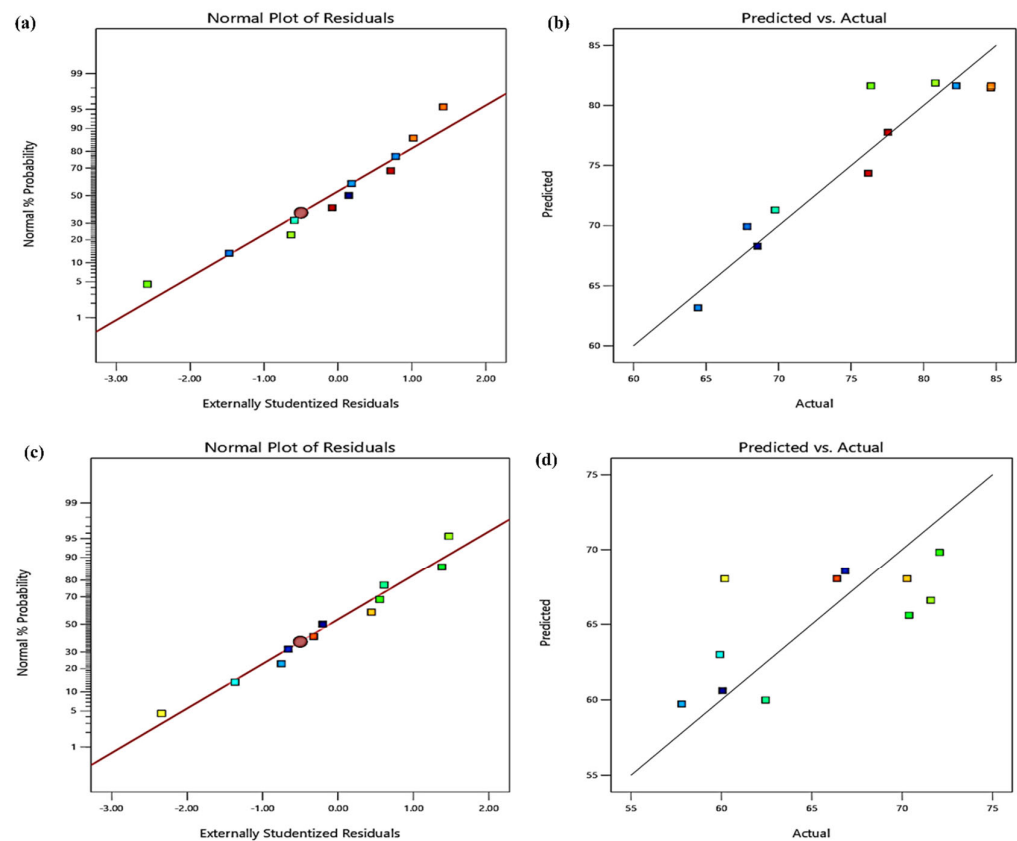


Figure 4. Plots of normal residuals and predicted versus actual plots of BASR for (a,b) BOD₅ and (c,d) COD removal.

3.4.4. ANOVA

ANOVA analysis was used to analyze the response surface of the quadratic model and to determine the model significance in addition to the individual terms engaged in terms of their p -values [43]. Fisher's test was used to determine the significance of each factor (HRT and MLSS) and their interactions. Table 8 summarizes the findings. For both responses, the p -values were lower than the F -values and <0.05 . This implies that both response prediction models are significant. As a result, it can be concluded that the model is able to fit the experimental data well, and that there is a connection among the variables and the BOD₅ and COD biosorption capacity. The model's F -values of 7.44 and 0.98 for BOD₅ and COD, respectively, indicate that the model is significant, with a mere 2.30% and 50.79% likelihood of this F -value occurring due to noise. As a result, the high F -value and low Prob $> F$ value of 0.0001 indicate the significance of Fisher's variance ratio, as well as confirming that the quadratic model possesses a high degree of fitness [44]. The ANOVA results provided the quadratic prediction models with a 95% confidence level for the elimination of BOD₅ and COD. In broad terms, lack of fit measures the likelihood that a model's projected value will fail to correspond to the actual value. As a result, if the model matches the data well, the lack of fit test will be insignificant. As shown in Table 8, no model had a substantial lack of fit for both BOD₅ (0.7512) and COD (0.4855) deletions. As a result, the ANOVA findings indicate that there is only a 0.01% probability that the F -values of the models will be significant due to noise. As a result, the lack of fit for the current system is negligible.

Table 8. Analysis of variance by RSM for BOD₅ and COD removal.

| | BOD ₅ | | | | | | COD | | | | | |
|----------------|------------------|----|-------------|---------|---------|-----------------|----------------|----|-------------|---------|---------|-----------------|
| | Sum of Squares | df | Mean Square | F-Value | p-Value | | Sum of Squares | df | Mean Square | F-Value | p-Value | |
| Model | 447.45 | 5 | 89.49 | 7.44 | 0.0230 | significant | 141.79 | 5 | 28.36 | 0.9817 | 0.0579 | significant |
| A-HRT | 155.04 | 1 | 155.04 | 12.88 | 0.0157 | | 47.21 | 1 | 47.21 | 1.63 | 0.0272 | |
| B-MLSS | 17.41 | 1 | 17.41 | 1.45 | 0.2829 | | 15.55 | 1 | 15.55 | 0.5384 | 0.4960 | |
| AB | 72.93 | 1 | 72.93 | 6.06 | 0.0571 | | 5.48 | 1 | 5.48 | 0.1896 | 0.6814 | |
| A ² | 69.60 | 1 | 69.60 | 5.78 | 0.0613 | | 69.50 | 1 | 69.50 | 2.41 | 0.1816 | |
| B ² | 78.64 | 1 | 78.64 | 6.53 | 0.0509 | | 0.0797 | 1 | 0.0797 | 0.0028 | 0.9601 | |
| Residual | 60.18 | 5 | 12.04 | | | | 144.43 | 5 | 28.89 | | | |
| Lack of Fit | 23.81 | 3 | 7.94 | 0.4364 | 0.7512 | not significant | 92.73 | 3 | 30.91 | 1.20 | 0.4855 | not significant |
| Pure Error | 36.37 | 2 | 18.18 | | | | 51.70 | 2 | 25.85 | | | |
| Cor Total | 507.63 | 10 | | | | | 286.22 | 10 | | | | |

3.4.5. Comparison and Fit Statistics

The quadratic model produced good statistical fit findings. Table 9 shows the appropriate precision ratios when comparing experimental values to anticipated values computed by the models. The suitable precision ratios of 2.5426 for BOD₅ and 7.3012 for COD for both models suggest that the models were appropriate for efficiently navigating the design space. Furthermore, the coefficients of variation (CV) for BOD₅ and COD removals were 8.23% and 4.58% (both 10%), indicating that the fitted models were dependable and precise. The coefficient of determination (R²), which evaluates the entire variation of predicted values to the mean, explains the general importance of each model in the present research. The coefficient of determination ought to be approximately 1 for models with strong prediction efficiency. Nevertheless, the effectiveness of a model cannot be determined only based on the coefficient of determination, because the value of R² increases with the total number of terms in the model independent of its statistical significance. The anticipated and modified R² values have a good correlation, while the Adeq precision for measuring the signal to noise ratio is excellent. In this study, the noise levels were 75.12% and 48.55% for BOD₅ and COD, respectively. The R² values in Table 9 indicate a high prediction efficiency for BOD₅ and COD elimination. To measure the predictive importance of the models, the value was compared to the modified R² value. BOD₅ and COD possessed R² and adjusted R² values of 0.4954 and 0.0092 and 0.8815 and 0.7629, respectively. These values are not far apart, implying that the model is suitable for explaining the correlation between the response and the inputs. Consequently, these data suggest that the quadratic model projected is in reasonable agreement with the experimental responses and can therefore be used. Considering these findings, it is possible to draw the conclusion that the model accurately represents the optimization of the removal of BOD₅ and COD from OPAH. A separate investigation delving into the removal of COD using CCD found comparable results.

Table 9. Fit statistics.

| | Std. Dev. | Mean | C.V.% | R ² | Adjusted R ² | Predicted R ² | Adeq Precision |
|------------------|-----------|-------|-------|----------------|-------------------------|--------------------------|----------------|
| BOD ₅ | 5.37 | 65.27 | 8.23 | 0.4954 | 0.0092 | 0.6415 | 2.5426 |
| COD | 3.47 | 75.73 | 4.58 | 0.8815 | 0.7629 | 0.4023 | 7.3012 |

Table 10 contains a description of the statistics adopted for the model comparison. The coefficient assessment of the variables and the effect of the variance inflation factor (VIF) were further investigated using variance analysis.

Table 10. Model comparison statistics.

| | PRESS | −2 Log Likelihood | BIC | AICc |
|------------------|--------|-------------------|-------|-------|
| BOD ₅ | 294.81 | 42.64 | 59.32 | 82.91 |
| COD | 756.04 | 59.54 | 73.93 | 92.54 |

3.4.6. Actual Factors and the Studentized Residuals

In Figure 5a, the plot of normal probability vs. Studentized residuals for BOD₅ and COD removal in the BASR reactor displays a linear trend, indicating the error distribution. As a result, according to the reaction parameters, the model can be deemed to correctly anticipate the reactions. Figure 5b, conversely, shows the plot of the anticipated value, indicating the suitability of the model and suitable data dispersion.

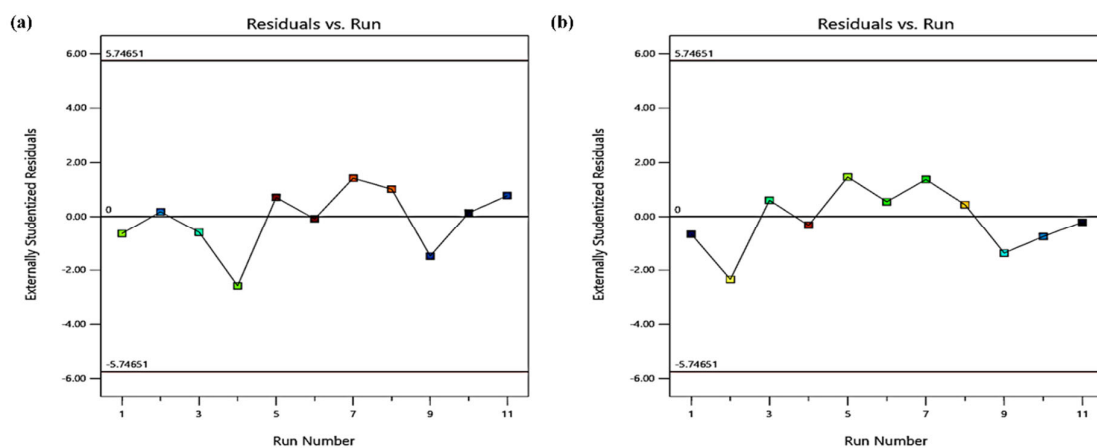


Figure 5. Plots of externally Studentized residuals vs. run number for BASR: (a) BOD₅; (b) COD.

The biosorption performance of OPAH is significantly impacted by all treatment parameters [45]. The response for a specific quantity of each factor can be forecast using the contents of Table 11, which represents the actual factors for BOD₅ and COD removals in the BASR reactor.

Table 11. The final equation in terms of actual factors.

| BOD ₅ Removal | = | COD Removal | = |
|--------------------------|-------------------|-------------|-------------------|
| −122.97316 | | +42.25474 | |
| +47.39965 | HRT | +29.60553 | HRT |
| +0.062552 | MLSS | −0.001044 | MLSS |
| −0.004270 | HRT × MLSS | −0.001170 | HRT × MLSS |
| −5.24158 | HRT ² | −5.23763 | HRT ² |
| −19.57158 | MLSS ² | −13.07368 | MLSS ² |

3.4.7. The Optimization Ramp and Desirability

Desirability charts and numerical ramps are the best tools for showcasing the optimal effluent treatment process, one of the key outcomes of RSM research. In this study, under ideal conditions, the results showed an optimal cumulative desirability of 68.8%, as shown in Figure 6a. The final stage in this inquiry was to use a numerical algorithm to discover the best solution. To optimize the response factors, numerical optimization ramps were utilized to acquire the best HRT and MLSS. Prospective targets were established to maximize the answers. Whereas a five-pluses method necessitates one goal being essential, all goals in this inquiry were equally significant; hence, the goal priority was determined to be three (3) pluses. Figure 6b shows that under ideal process conditions, the HRT was 1.885.35 d and MLSS was 4665.09 mg/L. The optimization ramp for the HRT and MLSS concentration

shows how desirable the dependent variables are [46]. According to the Design Expert software, version 13, the best values for BOD₅ and COD rates of removal were 80.76% and 68.15%, respectively.

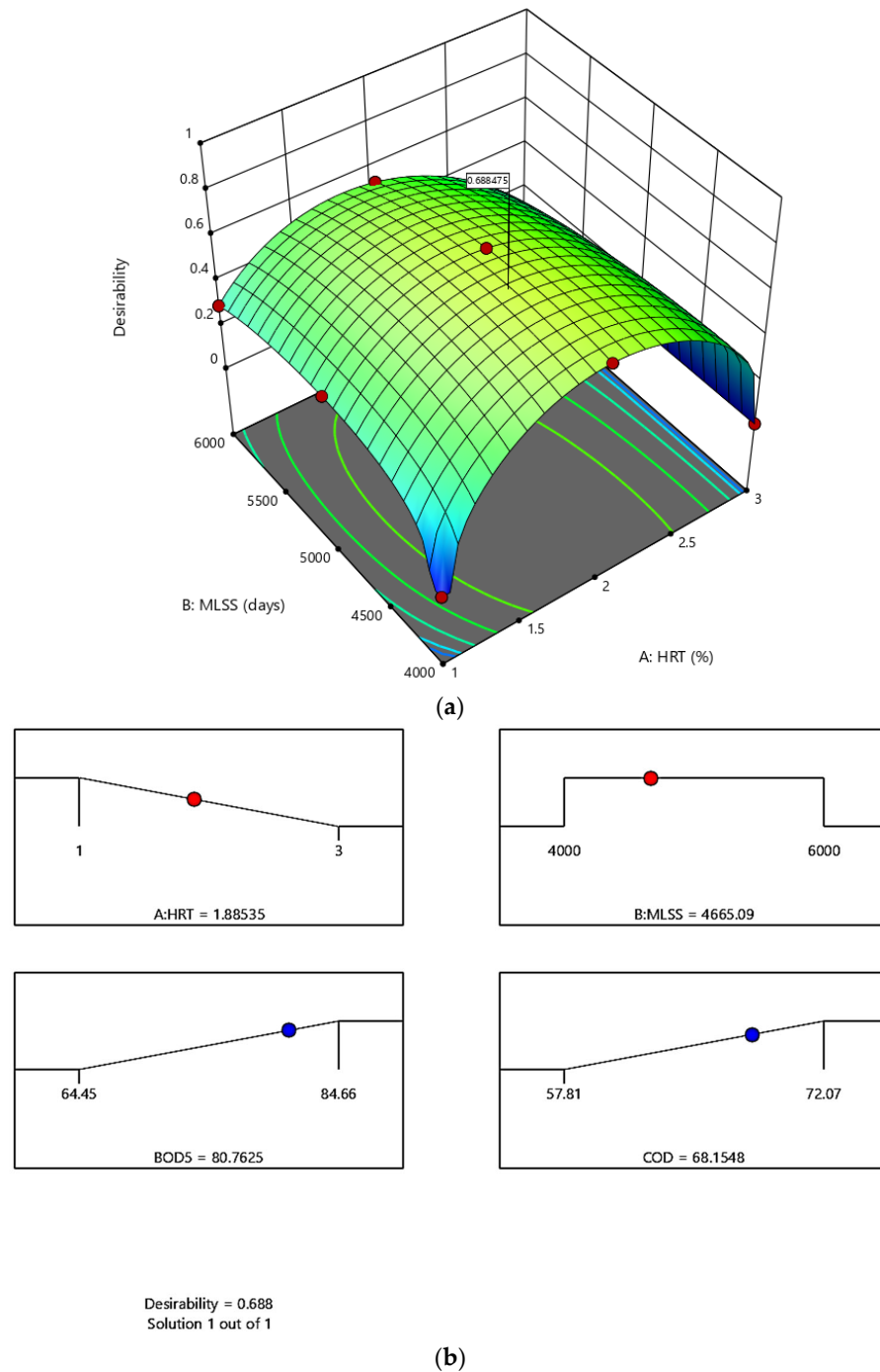


Figure 6. RSM optimization: (a) desirability and (b) ramps for the BASR system.

3.5. Biokinetic Models

3.5.1. First-Order Model

The first-order kinetic constant (C_1) for BOD₅ and COD removal in the bioreactor designs was determined in this study. Figure 7a,b display the experimental values for the $(N_i - N_0)/\mathcal{G}$ against N_0 terms. The effluents in the BASR had R^2 of 0.05533 and 0.09313 for BOD₅ and COD, respectively. The decreased R^2 values indicate that removal of first-order contaminants is less likely to occur following BOD₅ and COD removal in the bioreactors.

This outcome demonstrates that the first-order kinetics coefficients derived were incapable of being fitted precisely. These results clearly imply that the first-order model may not fully or adequately capture the dynamics of the bioreactor [47]. The B_1 in this study was a key factor when assessing the rate at which the concentrations of BOD₅ and COD decrease with time. The values of B_1 for BOD₅ and COD removal in the bioreactor were computed and determined to be 5.1438 per day and 4.3520 per day, respectively, based on a best-fit straight line for all starting concentrations. The B_1 value in first-order kinetics was small. It was found that the whole biomass concentration in the bioreactors varied from 8.03 to 9.11 g VSS/L on average.

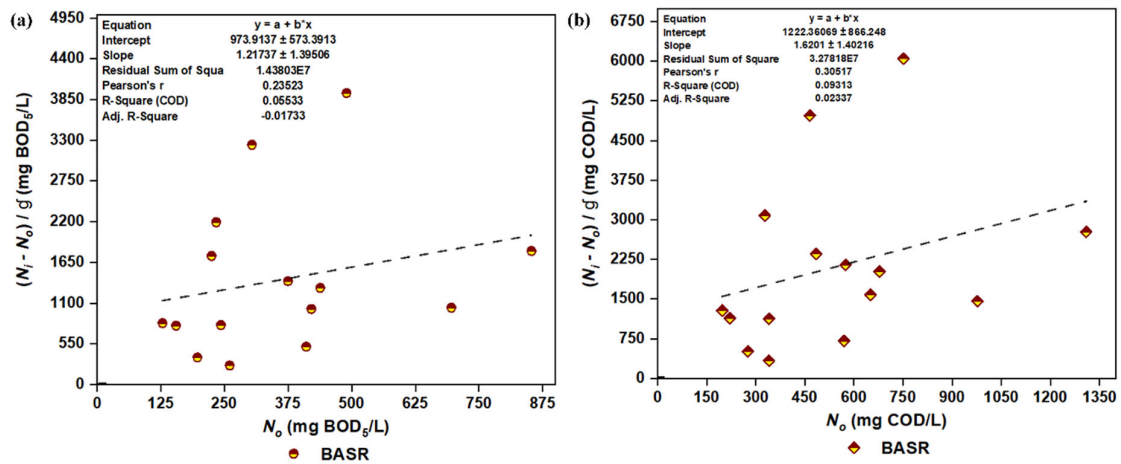


Figure 7. The first-order kinetic plot for (a) BOD₅ and (b) COD.

In the study reported in [27], wherein the height of the anaerobic reactors was adjusted from 0 to 160 cm, it was stated that no good determination coefficients were obtained using the first-order models ($R^2 = 0.3$). Nevertheless, when operated with an OLR of $5.28 \text{ kg m}^{-3} \text{ d}^{-1}$ and an HRT of 2.13 days, the reactor showed a median rate of removal of 78%. The removal kinetics was utilized for the SBR in steady states in [47]. According to the calculations, the first-order kinetic constants (B_1) for SBR1 and SBR2 were found to be 49.03 and 46.55 per day, respectively ($y = 61.09 \times 2.17$ and $R^2 = 0.9512$ and $y = 49.68 \times 2.50$ and $R^2 = 0.9421$ for the first- and second-batch reactors, respectively). The SRT of <4 d indicated that the first-order model was also appropriate, despite the Grau second-order model providing a superior description of substrate consumption, according to experimental data for wastewater treatment. In a related study, the first-order model of the bioreactor A showed that B_1 decreased with increasing beginning pollutant content. It was clear from the decreasing B_1 rate that the rate of pollutant removal was also declining.

3.5.2. The Grau Second-Order Model

By measuring the interconnection between $\frac{N_i}{N_o}$ versus N_o , as illustrated in Figure 8, a linear trend line can be utilized to calculate the kinetic parameters (j and k) that are employed in the Grau second-order model. Every line's slope and intercept are employed to demonstrate to what extent r and s is present in each line, respectively. The intercept and slope of the trend line are represented by j and k , respectively. The findings indicate that the values for j and k that correspond to the elimination of BOD₅ are, respectively, 0.073 and 1.49. For COD elimination, the comparable values are 0.058 and 1.32, respectively. The findings of this investigation support the values of j (0.053) and k (1.067) published in a different study [28]. The COD effluent concentration (N_o) from the BASR could be utilized to forecast process efficiency using these values for j and k . The s coefficient increases with increasing concentration; however, the j value has the reverse effect, according to the data. Consequently, the most favorable correlation coefficient values for BOD₅ and COD were obtained as $R^2 = 0.94041$ and $R^2 = 0.94278$, respectively.

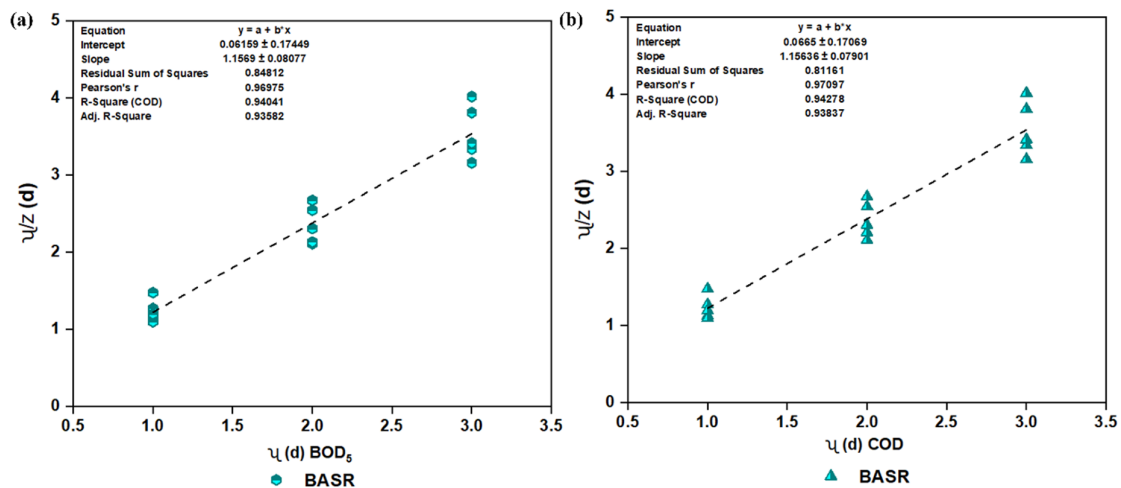


Figure 8. The second-order kinetic plot for (a) BOD₅, and (b) COD.

The Grau second-order kinetic model was used to determine the projected BOD₅ and COD concentrations in the effluent. It was found that for several days, the projected values diverged marginally from the experimental data, with the expected values being higher. The excessive and varying influent BOD₅ and COD concentrations fed into the reactor may have contributed to the significant variation among the experimental data and predictions between days 88 and 169, leading to an operational shortcoming [48]. Furthermore, the high OLRs of the influent had the potential to have increased head losses to the system, which could have contributed to the resulting high degree of variation among the predicted and experimental BOD₅ and COD values. These operational shortcomings were not considered in the Grau second-order model. The head losses to the system are caused by the particles building up on the pea gravel, which could choke the underdrain system.

Given each unit of microbe, the S_c in the unit of time reflects substrate removal. The value of S_c depends on the amounts of biomass and BOD₅ and COD in the influent of the reactor, and it increases with increasing substrate removal efficiency. The second-order model used in this work obtained constant value for S_c that were calculated to be 0.508 per day and 0.691 per day for BOD₅ and COD, respectively. The outcomes associated with this model are in line with the data for the removal of BOD₅ and COD. The model predicted that the substrate removal constant found fit to the spectrum of S_c values reported in other investigations. The features of the wastewater and the prevalent microorganisms in the granular sludge, however, may be the cause of the discrepancy in the values of the kinetic constants determined in this study in comparison with certain other studies.

3.5.3. The Modified Stover–Kincannon Kinetic Model

The constructed bioreactors in this study's kinetic reaction were also examined using the modified Stover–Kincannon model. The received experimental data were analyzed using the linearized model to find the values of the kinetic parameters [40]. The slope and intercept are comparable to the maximum rate of BOD₅ and COD elimination (C_t) and the saturation constant (F_y), respectively. The maximal amount of BOD₅ and COD that can be removed by organisms over time and the amount of BOD₅ and COD that can be removed by microorganisms over time are denoted by the constants F_y and C_t , respectively. When figuring out the reactor volume for various wastewater and flow rates, F_y and C_t play crucial roles [12]. Plotting $\frac{M_x}{P(N_i - N_0)}$ against $\frac{M_x}{PN_i}$ yielded the kinetic parameters C_t and F_y . The gradient is represented by $\frac{F_y}{C_t}$, while the intercept of the trend line is represented by $\frac{1}{C_t}$. The Stover model for BOD₅ and COD removal from AW in the bioreactor is shown in Figure 9a,b. The C_t values for BASR were 51.3 g/L.d and 56.5 g/L.d for BOD₅ and COD removal, respectively. The measured C_t and F_y values in the bioreactor system showed that the bioreactor had a higher utilization rate than certain alternative treatment systems [6].

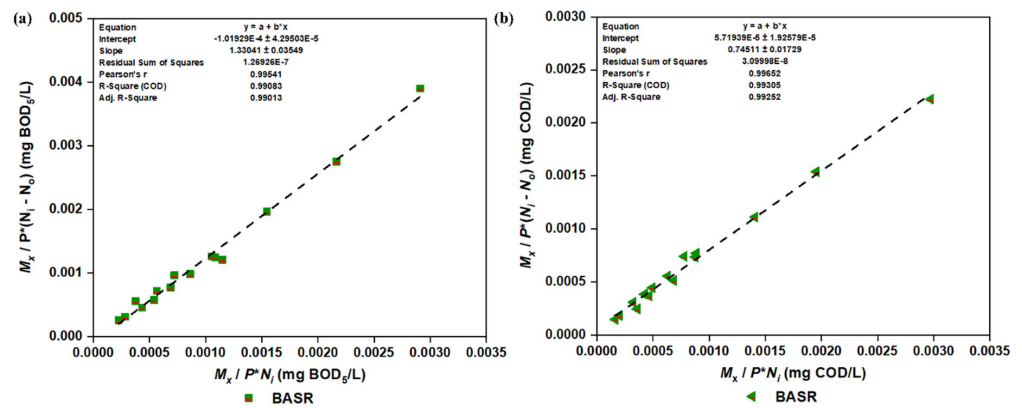


Figure 9. The modified Stover kinetic plot for (a) BOD₅ and (b) COD.

In general, it has been found that reactors exhibit greater kinetic constant parameters when treating easily biodegradable substrates, whereas more complicated and refractory components in the influent wastewater result in lower constant values. The high C_t and F_y results in this study demonstrate that the aerated submerged fixed-film bioreactor was highly capable of treating wastewater with high solubility levels [26]. To be more precise, it was demonstrated that the Stover model provides the greatest fit for the collected data. With the use of this model, precise estimates of biodegradable organic elimination could be established. The strong correlation coefficients required were attained. The results of this investigation demonstrated the excellent precision and usability of the hybrid bioreactor. Regarding pilot and large commercial applications, the kinetic correlations of the model might be utilized to predict the reactor volume and efficiency.

The kinetic constants for substrate removal provided in the literature review noted in Table 12 are contrasted with the values discovered here. Numerous scientists have used different substrates and reactors, and they have produced variable results in terms of kinetic constant values. After investigating the regression and biokinetic coefficients, the modified Stover–Kincannon and Grau second-order models offered a better description of the biokinetics of BOD₅ and COD removal. Although the microbial population in the reactor increased, the values of S_c significantly decreased as HRT decreased. The variation in the mean kinetic constants in different studies indicates that a variety of variables, including substrate concentration, substrate type, reactor configuration, operational circumstances, and the presence of microbial consortia, can significantly affect the values of kinetic coefficients.

Table 12. The biokinetic constants for BOD₅ and COD removal in bioreactors treating different agricultural wastewater.

| | | BOD ₅ | | | | | | | |
|--------------------------------|---|------------------|--------|-------------------|--------|-------------|---------------------------|---------------|------------|
| Wastewater | Reactor Type | Kinetic Model | | | | | | | Ref. |
| | | First-Order | | Grau Second-Order | | | Modified Stover–Kincannon | | |
| | | B_1 (1/d) | R^2 | j | k | S_c (1/d) | C_t (g/L/d) | F_y (g/L/d) | |
| Poultry industry effluent | Static Granular Bed Reactor (SGBR) | 0.425 | 0.9967 | 0.939 | 0.9619 | 76.4 | 8.05 | 5.19 | [48] |
| Fertilizer industry wastewater | Sequencing Batch Reactor (SBR) | 1.6 | 0.38 | 0.35 | 2.1 | 4.06 | 0.0627 | 0.0574 | [47] |
| Paper and pulp wastewater | Column-SBR | 1.334 | 0.802 | 1.214 | 0.945 | 0.0243 | 0.305 | 0.209 | [49] |
| Olive oil industry wastewater | SBR | 0.6148 | 0.9856 | 49.51 | 3.715 | 0.0872 | 0.0069 | 0.0871 | [50] |
| Palm oil mill effluent | Activated sludge bioreactor system (ASBS) | 0.077 | 0.6913 | 10.372 | 0.592 | 13.9 | 0.007 | 0.0628 | [51] |
| AW | Bench-scale activated sludge reactor (BASR) | 5.1438 | 0.5533 | 0.073 | 1.49 | 0.508 | 51.3 | 49.11 | This study |

Table 12. Cont.

| | | BOD ₅ | | | | | | | |
|------------------------------------|--|----------------------|----------------|-------------------|-------|----------------------|---------------------------|------------------------|------------|
| Wastewater | Reactor Type | Kinetic Model | | | | | | | Ref. |
| | | First-Order | | Grau Second-Order | | | Modified Stover–Kincannon | | |
| | | B ₁ (1/d) | R ² | j | k | S _c (1/d) | C _t (g/L/d) | F _y (g/L/d) | |
| COD | | | | | | | | | |
| Winery industry wastewater | Integrated fixed activated sludge (IFAS) | 87.2 | 0.59 | 0.053 | 0.778 | 0.384 | 47.8 | 62.6 | [52] |
| Pulp and paper industry wastewater | Anerobic-MBBR | 1.7 | 0.66 | 1.1 | 1.6 | 1.57 | 0.0203 | 0.0192 | [53] |
| Dairy industry | Moving bed biofilm reactor (MBBR) | 0.948 | 0.973 | 0.506 | 0.841 | 2.513 | 427 | 446 | [54] |
| Sugar-industry effluent | MBBR | 56.31 | 0.9742 | 0.9852 | 0.048 | 0.9852 | 37.61 | 40.8 | [55] |
| POME | SBR | 81.7 | 0.69 | 0.0852 | 0.773 | 0.38 | 63.7 | 64.0 | [56] |
| AW | BASR | 4.3520 | 0.0931 | 0.058 | 1.32 | 0.691 | 56.5 | 50.81 | This study |

3.6. Microbial Observation

A microscopic analysis was conducted to determine the presence of microorganisms in the activated sludge reactor. Based on the analysis, the presence of rotifers was found, and they were classified with respect to their microscopic morphology [1]. A visualization of the rotifers in the reactor is presented in Figure S3. The presence of Rotifers in the reactor proves that the reactor is in the pin floc zone. This also indicates that the reactor is running at a high Solid Retention Time (SRT) with a low Food-to-Microorganism (F/M) ratio. There were two types of microorganism found inside the aeration tank: *rotifers* and *oocysts*. Figure S3 shows that the sample contained *Phylum rotifera*, which is commonly found in freshwater. However, the presence of the rotifer in the wastewater reveals that the bench scale reactor has a sludge age value. Most rotifers are free-living organisms that can be easily found in numerous environments. These types do not cause any harm, and act as food for other predator organisms [42]. However, a few species of rotifer have been shown to be parasitic towards marine organisms and can cause harm to their host. Nevertheless, there are no reports stating parasitic rotifers have any effects on human beings.

Oocysts, as depicted in Figure S4, are disease-causing microorganisms that can mainly be found in the excrement of people infected with parasites such as *Cyclospora* and *Cryptosporidium*. This infection is caused by the consumption of contaminated water [57]. This microorganism may cause visible symptoms such as diarrhea, stomach cramps, nausea, and severe vomiting. This microorganism is commonly found in wastewater and has become a problem because the chlorination technique is ineffective at killing them.

4. Conclusions

In this study, the effectiveness of using OPAH as a biosorbent in a BASR system for the treatment of AW was evaluated. The process was optimized using RSM by setting the MLSS concentrations at 4000, 5000, and 6000 mg/L and the reactor running at 1–3 days HRT. The effectiveness of the treatment procedure was assessed based on the quantity of BOD₅, and COD removal. The results obtained demonstrated that the largest reductions in BOD₅ and COD were 84.66% and 72.07%, respectively. The greatest reductions in organic matter were accomplished with a 2-day HRT and an MLSS concentration of 5000 mg/L. The BASR good removal efficiency could be attributed to the availability of sufficient ammonia oxidizing bacteria (AOB) substrates during a longer retention period. The specified and response models for *p*-values < 5%, as well as the quadratic models, were demonstrated to be significant during RSM optimization. The study also examined the various processes

using three different biokinetic models and proved the modified Stover–Kincannon to be the best, with high R^2 values of 0.9908 and 0.9931 being attained for BOD_5 and COD, respectively. Therefore, in this study, it is concluded that using agricultural waste materials to develop a biosorbent has the potential to be an inventive way of removing BOD_5 and COD from AW.

Supplementary Materials: The following supporting information can be downloaded at: <https://www.mdpi.com/article/10.3390/agriculture13081531/s1>, Figure S1: (a) Palm oil fruit bunches (PFB); (b) Oil palm activated hydrochar (OPAH); Figure S2: Schematic diagram of BASR set-up; Figure S3: Images of Rotifer captured through microscope; Figure S4: Image of Oocyst captured through microscope.

Author Contributions: Conceptualization, A.H.J.; Methodology, A.H.J., F.M.B. and N.M.S.; Software, I.M.L., A.K.U., N.S.A.Y., A.H.B. and H.Y.H.; Validation, N.S.A.Y.; Formal analysis, A.H.B.; Investigation, N.S.A.Y.; Resources, F.M.B., A.K.U., A.H.B. and N.M.S.; Data curation, I.M.L., A.K.U., A.H.B., H.Y.H. and N.M.S.; Writing—original draft, A.H.J.; Writing—review & editing, A.H.J. and F.M.B.; Visualization, A.K.U. and H.Y.H.; Supervision, I.M.L.; Project administration, F.M.B. and I.M.L.; Funding acquisition, N.M.S. All authors have read and agreed to the published version of the manuscript.

Funding: This research was funded by the Scientific Research Deanship at University of Ha'il, Saudi Arabia under the project with grant number RG-20 220 and Universiti Teknologi PETRONAS (UTP), Malaysia.

Institutional Review Board Statement: Not applicable.

Data Availability Statement: The data presented in this study are available from the corresponding authors upon request.

Acknowledgments: The authors would like to acknowledge the Scientific Research Deanship at University of Ha'il, Saudi Arabia. Additionally, the authors express their gratitude to Universiti Teknologi PETRONAS (UTP), Malaysia.

Conflicts of Interest: The authors declare no conflict of interest.

References

1. Hernández, D.; Riaño, B.; Coca, M.; García-González, M. Treatment of agro-industrial wastewater using microalgae–bacteria consortium combined with anaerobic digestion of the produced biomass. *Bioresour. Technol.* **2013**, *135*, 598–603. [\[CrossRef\]](#)
2. Abdullahi, S.S.; Birniwa, A.H.; Mohammad, R.E.; Mamman, S.; Chadi, A.S. Impact of fibre reinforced polyester composites on tensile strength of baobab (*Adansonia digitata*) stem. *CaJoST* **2020**, *2*, 94–100.
3. Martinez-Burgos, W.J.; Sydney, E.B.; Medeiros, A.B.P.; Magalhães, A.I.; de Carvalho, J.C.; Karp, S.G.; de Souza Vandenberghe, L.P.; Letti, L.A.J.; Soccol, V.T.; de Melo Pereira, G.V. Agro-industrial wastewater in a circular economy: Characteristics, impacts and applications for bioenergy and biochemicals. *Bioresour. Technol.* **2021**, *341*, 125795. [\[CrossRef\]](#)
4. Baloo, L.; Isa, M.H.; Sapari, N.B.; Jagaba, A.H.; Wei, L.J.; Yavari, S.; Razali, R.; Vasu, R. Adsorptive removal of methylene blue and acid orange 10 dyes from aqueous solutions using oil palm wastes-derived activated carbons. *Alex. Eng. J.* **2021**, *60*, 5611–5629. [\[CrossRef\]](#)
5. Birniwa, A.H.; Mahmud, H.N.M.E.; Abdullahi, S.S.A.; Habibu, S.; Jagaba, A.H.; Ibrahim, M.N.M.; Ahmad, A.; Alshammari, M.B.; Parveen, T.; Umar, K. Adsorption behavior of methylene blue cationic dye in aqueous solution using polypyrrole-polyethylenimine nano-adsorbent. *Polymers* **2022**, *14*, 3362. [\[CrossRef\]](#) [\[PubMed\]](#)
6. Birniwa, A.H.; Abdullahi, S.S.A.; Ali, M.; Mohammad, R.E.A.; Jagaba, A.H.; Amran, M.; Avudaiappan, S.; Maureira-Carsalade, N.; Flores, E.I.S. Recent Trends in Treatment and Fabrication of Plant-Based Fiber-Reinforced Epoxy Composite: A Review. *J. Compos. Sci.* **2023**, *7*, 120. [\[CrossRef\]](#)
7. Kumar, M.; Ambika, S.; Hassani, A.; Nidheesh, P. Waste to catalyst: Role of agricultural waste in water and wastewater treatment. *Sci. Total Environ.* **2023**, *858*, 159762. [\[CrossRef\]](#)
8. Al-Sabaeei, A.M.; Al-Fakih, A.; Noura, S.; Yaghoubi, E.; Alaloul, W.; Al-Mansob, R.A.; Khan, M.I.; Yaro, N.S.A. Utilization of palm oil and its by-products in bio-asphalt and bio-concrete mixtures: A review. *Constr. Build. Mater.* **2022**, *337*, 127552. [\[CrossRef\]](#)
9. Muhammad, S.; Yahya, E.B.; Abdul Khalil, H.; Marwan, M.; Albadn, Y.M. Recent Advances in Carbon and Activated Carbon Nanostructured Aerogels Prepared from Agricultural Wastes for Wastewater Treatment Applications. *Agriculture* **2023**, *13*, 208. [\[CrossRef\]](#)

10. Usman, A.; Aris, A.; Labaran, B.; Darwish, M.; Jagaba, A. Effect of Calcination Temperature on the Morphology, Crystallinity, and Photocatalytic Activity of ZnO/TiO₂ in Selenite Photoreduction from Aqueous Phase. *J. New Mater. Electrochem. Syst.* **2022**, *25*, 251–258. [[CrossRef](#)]
11. Umaru, I.; Alhaji, M.M.; Alhassan, M.; Adejumo, T.E.; Alkali, B.; Birniwa, A.H.; Jagaba, A.H. Development of Innovative Plate Load Testing Equipment for In-Situ Saturated Clays Soils. *Geotechnics* **2023**, *3*, 142–160. [[CrossRef](#)]
12. Abdullahi, S.S.A.; Musa, H.; Habibu, S.; Birniwa, A.H.; Mohammad, R.E.A. Comparative study and dyeing performance of as-synthesized azo heterocyclic monomeric, polymeric, and commercial disperse dyes. *Turk. J. Chem.* **2022**, *46*, 1841–1852. [[CrossRef](#)]
13. Nogueira, G.D.; Duarte, C.R.; Barrozo, M.A. Hydrothermal carbonization of acerola (*Malpighia emarginata* DC) wastes and its application as an adsorbent. *Waste Manag.* **2019**, *95*, 466–475. [[CrossRef](#)] [[PubMed](#)]
14. Yaro, N.S.A.; Sutanto, M.H.; Habib, N.Z.; Usman, A.; Kaura, J.M.; Murana, A.A.; Birniwa, A.H.; Jagaba, A.H. A Comprehensive Review of Biochar Utilization for Low-Carbon Flexible Asphalt Pavements. *Sustainability* **2023**, *15*, 6729. [[CrossRef](#)]
15. Soffian, M.S.; Halim, F.Z.A.; Aziz, F.; Rahman, M.A.; Amin, M.A.M.; Chee, D.N.A. Carbon-based material derived from biomass waste for wastewater treatment. *Environ. Adv.* **2022**, *9*, 100259. [[CrossRef](#)]
16. Yaro, N.S.A.; Sutanto, M.H.; Habib, N.Z.; Napihah, M.; Usman, A.; Jagaba, A.H.; Al-Sabaeei, A.M. Modeling and optimization of asphalt content, waste palm oil clinker powder and waste rice straw ash for sustainable asphalt paving employing response surface methodology: A pilot study. *Clean. Mater.* **2023**, *8*, 100187. [[CrossRef](#)]
17. Dehghani, M.H.; Yetilmezsoy, K.; Salari, M.; Heidarinejad, Z.; Yousefi, M.; Sillanpää, M. Adsorptive removal of cobalt (II) from aqueous solutions using multi-walled carbon nanotubes and γ -alumina as novel adsorbents: Modelling and optimization based on response surface methodology and artificial neural network. *J. Mol. Liq.* **2020**, *299*, 112154. [[CrossRef](#)]
18. Kohzadi, S.; Marzban, N.; Libra, J.A.; Bundschuh, M.; Maleki, A. Removal of RhB from water by Fe-modified hydrochar and biochar—An experimental evaluation supported by genetic programming. *J. Mol. Liq.* **2023**, *369*, 120971. [[CrossRef](#)]
19. Milkey, R. Potassium bromide method of infrared sampling. *Anal. Chem.* **1958**, *30*, 1931–1933. [[CrossRef](#)]
20. ASTM E871-82; Standard Test Method for MOISTURE Analysis of Particulate Wood Fuels. American Society for Testing and Materials (ASTM): Philadelphia, PA, USA, 2006.
21. ASTM E1755-01; Standard Test Method for Ash in Biomass—ASTM Bioenergy and Industrial Chemicals from Biomass. ASTM International: West Conshohocken, PA, USA, 2015.
22. ASTM D3176-09; Standard Practice for Ultimate Analysis of Coal and Coke. ASTM International: West Conshohocken, PA, USA, 2009.
23. ASTM D4809-00; Standard Test Method for Heat of Combustion of Liquid Hydrocarbon Fuels by Bomb Calorimeter (Precision Method). ASTM International: West Conshohocken, PA, USA, 2013.
24. Yaro, N.S.A.; Napihah, M.B.; Sutanto, M.H.; Usman, A.; Saeed, S.M. Modeling and optimization of mixing parameters using response surface methodology and characterization of palm oil clinker fine modified bitumen. *Constr. Build. Mater.* **2021**, *298*, 123849. [[CrossRef](#)]
25. Usman, A.; Sutanto, M.H.; Napihah, M.; Zoorob, S.E.; Yaro, N.S.A.; Khan, M.I. Comparison of performance properties and prediction of regular and gamma-irradiated granular waste polyethylene terephthalate modified asphalt mixtures. *Polymers* **2021**, *13*, 2610. [[CrossRef](#)] [[PubMed](#)]
26. Tadda, M.A.; Gouda, M.; Shitu, A.; Yu, Q.; Zhao, X.; Ying, L.; Zhu, S.; Liu, D. Baobab fruit powder promotes denitrifiers' abundance and improves poly (butylene succinate) biodegradation for a greener environment. *J. Environ. Chem. Eng.* **2023**, *11*, 109654. [[CrossRef](#)]
27. Shitu, A.; Chen, W.; Tadda, M.A.; Zhang, Y.; Ye, Z.; Liu, D.; Zhu, S.; Zhao, J. Enhanced aquaculture wastewater treatment in a biofilm reactor filled with sponge/ferrous oxalate/biochar composite (Sponge-C2FeO4@NBC) biocarriers: Performance and mechanism. *Chemosphere* **2023**, *330*, 138772. [[CrossRef](#)] [[PubMed](#)]
28. Tadda, M.A.; Altaf, R.; Gouda, M.; Rout, P.R.; Shitu, A.; Ye, Z.; Zhu, S.; Liu, D. Impact of Saddle-Chips biocarrier on treating mariculture wastewater by moving bed biofilm reactor (MBBR): Mechanism and kinetic study. *J. Environ. Chem. Eng.* **2021**, *9*, 106710. [[CrossRef](#)]
29. Kankia, M.U.; Baloo, L.; Danlami, N.; Mohammed, B.S.; Haruna, S.; Abubakar, M.; Jagaba, A.H.; Sayed, K.; Abdulkadir, I.; Salihi, I.U. Performance of Fly Ash-Based Inorganic Polymer Mortar with Petroleum Sludge Ash. *Polymers* **2021**, *13*, 4143. [[CrossRef](#)] [[PubMed](#)]
30. Abdullahi, S.S.A.; Musa, H.; Habibu, S.; Birniwa, A.H.; Mohammad, R.E.A. Facile synthesis and dyeing performance of some disperse monomeric and polymeric dyes on nylon and polyester fabrics. *Bull. Chem. Soc. Ethiop.* **2021**, *35*, 485–497. [[CrossRef](#)]
31. Birniwa, A.H.; Abdullahi, S.S.A.; Yakasai, M.Y.; Ismaila, A. Studies on physico-mechanical behaviour of kenaf/glass fiber reinforced epoxy hybrid composites. *Bull. Chem. Soc. Ethiop.* **2021**, *35*, 171–184. [[CrossRef](#)]
32. Muhamad Ng, S.N.; Idrus, S.; Ahsan, A.; Tuan Mohd Marzuki, T.N.; Mahat, S.B. Treatment of wastewater from a food and beverage industry using conventional wastewater treatment integrated with membrane bioreactor system: A pilot-scale case study. *Membranes* **2021**, *11*, 456. [[CrossRef](#)]
33. Birniwa, A.H.; Abubakar, A.S.; Huq, A.O.; Mahmud, H.N.M.E. Polypyrrole-polyethyleneimine (PPy-PEI) nanocomposite: An effective adsorbent for nickel ion adsorption from aqueous solution. *J. Macromol. Sci. Part A* **2021**, *58*, 206–217. [[CrossRef](#)]

34. Satyawali, Y.; Balakrishnan, M. Wastewater treatment in molasses-based alcohol distilleries for COD and color removal: A review. *J. Environ. Manag.* **2008**, *86*, 481–497. [[CrossRef](#)]
35. Leiviskä, T.; Nurmesniemi, H.; Pöykiö, R.; Rämö, J.; Kuokkanen, T.; Pellinen, J. Effect of biological wastewater treatment on the molecular weight distribution of soluble organic compounds and on the reduction of BOD, COD and P in pulp and paper mill effluent. *Water Res.* **2008**, *42*, 3952–3960. [[CrossRef](#)] [[PubMed](#)]
36. Birniwa, A.H.; Mohammad, R.E.A.; Ali, M.; Rehman, M.F.; Abdullahi, S.S.A.; Eldin, S.M.; Mamman, S.; Sadiq, A.C.; Jagaba, A.H. Synthesis of Gum Arabic Magnetic Nanoparticles for Adsorptive Removal of Ciprofloxacin: Equilibrium, Kinetic, Thermodynamics Studies, and Optimization by Response Surface Methodology. *Separations* **2022**, *9*, 322. [[CrossRef](#)]
37. Usman, S.; Yakasai, H.M.; Gimba, M.Y.; Shehu, D.; Jagaba, A.H. Anthracene degradation by *Achromobacter xylosoxidans* strain BUK_BTEG6 isolated from petrochemical contaminated soil. *Case Stud. Chem. Environ. Eng.* **2023**, *8*, 100418. [[CrossRef](#)]
38. Lawal, I.; Ndagi, A.; Mohammed, A.; Saleh, Y.; Shuaibu, A.; Hassan, I.; Abubakar, S.; Soja, U.; Jagaba, A. Proximate analysis of waste-to-energy potential of municipal solid waste for sustainable renewable energy generation. *Ain Shams Eng. J.* **2023**, 102357. [[CrossRef](#)]
39. Lawal, I.M.; Bertram, D.; White, C.J.; Jagaba, A.H.; Hassan, I.; Shuaibu, A. Multi-criteria performance evaluation of gridded precipitation and temperature products in data-sparse regions. *Atmosphere* **2021**, *12*, 1597. [[CrossRef](#)]
40. Saeed, A.A.H.; Harun, N.Y.; Sufian, S.; Bilad, M.R.; Zakaria, Z.Y.; Jagaba, A.H.; Ghaleb, A.A.S.; Mohammed, H.G. Pristine and magnetic kenaf fiber biochar for Cd²⁺ adsorption from aqueous solution. *Int. J. Environ. Res. Public Health* **2021**, *18*, 7949. [[CrossRef](#)]
41. Abioye, K.J.; Harun, N.Y.; Sufian, S.; Yusuf, M.; Kamyab, H.; Hassan, M.A.; Jagaba, A.H.; Sikiru, S.; Ubaidullah, M.; Pandit, B. Regulation of ash slagging behavior of palm oil decanter cake by alum sludge addition. *Chemosphere* **2023**, *330*, 138452. [[CrossRef](#)]
42. Birniwa, A.; Abdullahi, S. Study on physico-mechanical behaviour of acacia nilotica (gum tree) and glass fiber blend reinforced epoxy resin composite. *ChemSearch J.* **2019**, *10*, 46–53.
43. Zahrim, A.; Nasimah, A.; Hilal, N. Coagulation/flocculation of lignin aqueous solution in single stage mixing tank system: Modeling and optimization by response surface methodology. *J. Environ. Chem. Eng.* **2015**, *3*, 2145–2154. [[CrossRef](#)]
44. Kankia, M.U.; Baloo, L.; Danlami, N.; Samahani, W.N.; Mohammed, B.S.; Haruna, S.; Jagaba, A.H.; Abubakar, M.; Ishak, E.A.; Sayed, K. Optimization of Cement-Based Mortar Containing Oily Sludge Ash by Response Surface Methodology. *Materials* **2021**, *14*, 6308. [[CrossRef](#)]
45. Asfaram, A.; Ghaedi, M.; Agarwal, S.; Tyagi, I.; Gupta, V.K. Removal of basic dye Auramine-O by ZnS: Cu nanoparticles loaded on activated carbon: Optimization of parameters using response surface methodology with central composite design. *RSC Adv.* **2015**, *5*, 18438–18450. [[CrossRef](#)]
46. Saeed, A.A.H.; Harun, N.Y.; Sufian, S.; Bilad, M.R.; Nufida, B.A.; Ismail, N.M.; Zakaria, Z.Y.; Jagaba, A.H.; Ghaleb, A.A.S.; Al-Dhawi, B.N.S. Modeling and optimization of biochar based adsorbent derived from Kenaf using response surface methodology on adsorption of Cd²⁺. *Water* **2021**, *13*, 999. [[CrossRef](#)]
47. Amin, M.M.; Khiadani, M.H.; Fatehizadeh, A.; Taheri, E. Validation of linear and non-linear kinetic modeling of saline wastewater treatment by sequencing batch reactor with adapted and non-adapted consortiums. *Desalination* **2014**, *344*, 228–235. [[CrossRef](#)]
48. Basitere, M.; Njoya, M.; Rinqest, Z.; Ntwampe, S.K.O.; Sheldon, M. Performance evaluation and kinetic parameter analysis for static granular bed reactor (SGBR) for treating poultry slaughterhouse wastewater at mesophilic condition. *Water Pract. Technol.* **2019**, *14*, 259–268. [[CrossRef](#)]
49. Khan, N.A.; Khan, S.U.; Islam, D.T.; Ahmed, S.; Farooqi, I.H.; Isa, M.H.; Hussain, A.; Changani, F.; Dhingra, A. Performance evaluation of column-SBR in paper and pulp wastewater treatment: Optimization and bio-kinetics. *Desalin Water Treat.* **2019**, *156*, 204–219. [[CrossRef](#)]
50. Esteves, B.M.; Morales-Torres, S.; Maldonado-Hódar, F.J.; Madeira, L.M. Fitting biochars and activated carbons from residues of the olive oil industry as supports of Fe-catalysts for the heterogeneous Fenton-like treatment of simulated olive mill wastewater. *Nanomaterials* **2020**, *10*, 876. [[CrossRef](#)]
51. Chan, Y.J.; Chong, M.F.; Law, C.L. Performance and kinetic evaluation of an integrated anaerobic–aerobic bioreactor in the treatment of palm oil mill effluent. *Environ. Technol.* **2017**, *38*, 1005–1021. [[CrossRef](#)]
52. Zinatizadeh, A.; Ghaytooli, E. Simultaneous nitrogen and carbon removal from wastewater at different operating conditions in a moving bed biofilm reactor (MBBR): Process modeling and optimization. *J. Taiwan Inst. Chem. Eng.* **2015**, *53*, 98–111. [[CrossRef](#)]
53. Tsang, Y.F.; Chua, H.; Sin, S.; Tam, C. A novel technology for bulking control in biological wastewater treatment plant for pulp and paper making industry. *Biochem. Eng. J.* **2006**, *32*, 127–134. [[CrossRef](#)]
54. Santos, A.D.; Martins, R.C.; Quinta-Ferreira, R.M.; Castro, L.M. Moving bed biofilm reactor (MBBR) for dairy wastewater treatment. *Energy Rep.* **2020**, *6*, 340–344. [[CrossRef](#)]
55. Faridnasr, M.; Ghanbari, B.; Sassani, A. Optimization of the moving-bed biofilm sequencing batch reactor (MBSBR) to control aeration time by kinetic computational modeling: Simulated sugar-industry wastewater treatment. *Bioresour. Technol.* **2016**, *208*, 149–160. [[CrossRef](#)] [[PubMed](#)]

56. Fulazzaky, M.A.; Nuid, M.; Aris, A.; Muda, K. Kinetics and mass transfer studies on the biosorption of organic matter from palm oil mill effluent by aerobic granules before and after the addition of *Serratia marcescens* SA30 in a sequencing batch reactor. *Process Saf. Environ. Prot.* **2017**, *107*, 259–268. [[CrossRef](#)]
57. Yaro, N.S.A.; Sutanto, M.H.; Baloo, L.; Habib, N.Z.; Usman, A.; Ahmad, A.; Yousafzai, A.K.; Birniwa, A.H.; Jagaba, A.H.; Noor, A. A Comprehensive Overview of the Utilization of Recycled Waste Materials and Technologies in Asphalt Pavements: Towards Environmental and Sustainable Low-Carbon Roads. *Processes* **2023**, *11*, 2095. [[CrossRef](#)]

Disclaimer/Publisher’s Note: The statements, opinions and data contained in all publications are solely those of the individual author(s) and contributor(s) and not of MDPI and/or the editor(s). MDPI and/or the editor(s) disclaim responsibility for any injury to people or property resulting from any ideas, methods, instructions or products referred to in the content.